Distributed Online VAR Control for Unbalanced Distribution Networks with Photovoltaic Generation

Jiayong Li, *Member, IEEE*, Chengying Liu, Mohammad E. Khodayar, *Senior Member, IEEE*, Ming-hao Wang, *Member, IEEE*, Zhao Xu, *Senior Member, IEEE*, Bin Zhou, *Senior Member, IEEE*, Canbing Li, *Senior Member, IEEE*

***Abstract*—The unbalanced nature of the distribution networks (DNs) and communication asynchrony pose considerable challenges to the distributed voltage regulation. In this paper, two distributed voltage control algorithms are proposed to overcome these challenges in multiphase unbalanced DNs. The proposed algorithms can be leveraged in online implementations to cope with the fast-varying system operating conditions. By adopting the linearized multiphase DistFlow model, the voltage control problem is formulated as a convex quadratic programming problem for which a synchronous distributed algorithm is developed based on the dual ascent method. To account for communication delays, an asynchronous distributed algorithm is proposed evolving from the synchronous one by incorporating an event-triggered communication protocol. Furthermore, closed-form solutions to the optimization subproblems are derived to enhance the computational efficiency, and communication complexity is reduced significantly to the extent that only neighborhood information exchange is required. Finally, the convergence of the proposed algorithms to the global optimality is established analytically. Numerical tests on the IEEE 123-bus network not only corroborate that our proposed algorithms are more efficient in eliminating voltage violations and minimizing network loss compared with two benchmarks but also validate their effectiveness for online implementations.**

***Index Terms*—Distribution networks, multiphase unbalance, online voltage control, synchronous and asynchronous distributed algorithms.**

NOMENCLATURE

Indices and sets:

i	Index of buses/lines
ϕ	Index of phases
π_i	Parent bus of bus i
C_i	Set of child buses of bus i

Parameters:

$\mathbf{A}^0$	Line-bus incidence matrix
$\mathbf{A}$	Reduced line-bus incidence matrix
$\mathbf{a}_0$	The first column of $\mathbf{A}^0$
$\mathbf{z}_i$	Impedance matrix of line i
$\mathbf{r}_i/\mathbf{x}_i$	Resistance/Reactance matrices of line i
$\boldsymbol{\alpha}$	Auxiliary complex vector defined as $\boldsymbol{\alpha} := [1\ \alpha\ \alpha^2]^\top$, where $\alpha = e^{-j(2\pi/3)}$
$\tilde{\mathbf{z}}_i/\tilde{\mathbf{r}}_i$	Auxiliary impedance/resistance matrices of line i defined as $\tilde{\mathbf{z}}_i := \text{diag}(\boldsymbol{\alpha}^*)\mathbf{z}_i\text{diag}(\boldsymbol{\alpha})$ and $\tilde{\mathbf{r}}_i := \text{diag}(\boldsymbol{\alpha})\mathbf{r}_i\text{diag}(\boldsymbol{\alpha}^*)$
$\mathbf{M}$	Auxiliary matrix defined as $\mathbf{M} := \mathbf{A}^{-\top} \otimes \mathbf{I}_3$, where $\mathbf{I}_3$ is the 3-dimensional identity matrix
$\mathbf{R}/\mathbf{X}$	Matrices that relates nodal active/reactive power injections to squared nodal voltage magnitudes, defined as $\mathbf{R} := 2\mathbf{M}^\top\text{bdiag}\left([\text{Re}(\tilde{\mathbf{z}}_i)]\right)\mathbf{M}$ and $\mathbf{X} := 2\mathbf{M}^\top\text{bdiag}\left([\text{Im}(\tilde{\mathbf{z}}_i)]\right)\mathbf{M}$
$\tilde{\mathbf{R}}_r/\tilde{\mathbf{R}}_x$	Auxiliary matrices for calculating network loss, defined as $\tilde{\mathbf{R}}_r := \mathbf{M}^\top\text{bdiag}\left([\text{Re}(\tilde{\mathbf{r}}_i)]\right)\mathbf{M}$ and $\tilde{\mathbf{R}}_x := \mathbf{M}^\top\text{bdiag}\left([\text{Im}(\tilde{\mathbf{r}}_i)]\right)\mathbf{M}$
$\overline{q}_{i,\phi}/\underline{q}_{i,\phi}$	Upper/Lower bound of reactive power injection at node (i,ϕ)
$\overline{\alpha}_i/\underline{\alpha}_i$	Step sizes for updating $\overline{\boldsymbol{\mu}}_i/\underline{\boldsymbol{\mu}}_i$
$\overline{\gamma}_i/\underline{\gamma}_i$	Step sizes for updating $\overline{\boldsymbol{\omega}}_i/\underline{\boldsymbol{\omega}}_i$
K_i	Line parameter of line i defined as $K_i := \text{Re}(\tilde{\mathbf{r}}_i)^{-1}\text{Im}(\tilde{\mathbf{z}}_i)^\top$
$\mathbf{B}_{ij}$	The (i,j)th block of $\tilde{\mathbf{R}}_r^{-1}$

Variables:

$\mathbf{S}_i/\mathbf{P}_i$	Vectors of complex/active power flow on line i
$\mathbf{v}_i$	Vector of squared voltage magnitudes at bus i
$\mathbf{s}_i$	Vector of complex power injection at bus i
$\mathbf{p}/\mathbf{q}$	Vectors of active/reactive power injections in DN
$\overline{\boldsymbol{\mu}}_i/\underline{\boldsymbol{\mu}}_i$	Dual variables associated with voltage constraints
$\overline{\boldsymbol{\omega}}_i/\underline{\boldsymbol{\omega}}_i$	Dual variables associated with reactive power limit constraints
$\tilde{\mathbf{P}}_i$	Vector of auxiliary active power flow on line i defined as $\tilde{\mathbf{P}}_i := \text{Re}(\tilde{\mathbf{r}}_i)^{-1}\text{Im}(\tilde{\mathbf{r}}_i)\mathbf{P}_i$

I. INTRODUCTION

THE widespread adoption of distribution energy resources (DERs) such as solar photovoltaic (PV) generation can cause frequent and severe voltage violations in the distribution networks (DNs) [1]–[3]. Leveraging the advantages of PV inverters for providing reactive power (VAR) support is a promising solution to resolve this issue [4]–[6]. However, a key

This work is supported in part by the National Natural Science Foundation of China under Grant No. 51907056, in part by the U.S. Department of Energy's Solar Energy Technologies Office under Grant CPS34228, and in part by the National Science Foundation under Grant ECCS-1710923.

J. Li is with the College of Electrical and Information Engineering, Hunan University, Changsha 410082, China, and also with the Department of Electrical and Computer Engineering, Southern Methodist University, Dallas, TX 75275 USA (email: j-y.li@connect.polyu.hk).

C. Liu and B. Zhou are with the College of Electrical and Information Engineering, Hunan University, Changsha 410082, China (emails: liu68@hnu.edu.cn, binzhou@hnu.edu.cn).

M. E. Khodayar is with the Department of Electrical and Computer Engineering, Southern Methodist University, Dallas, TX 75275 USA (email: mkhodayar@smu.edu).

M. Wang and Z. Xu are with the Department of Electrical Engineering, The Hong Kong Polytechnic University, Hung Hom, Hong Kong (emails: minghao.wang@polyu.edu.hk, eezhaoxu@polyu.edu.hk).

C. Li is with the Department of Electrical Engineering, Shanghai Jiao Tong University, Shanghai 200240, China (email: licanbing@sjtu.edu.cn)

challenge for coordinating multiple dispersed PV systems to perform fast and flexible voltage regulation is to handle various practical operational issues, such as three-phase unbalanced demand and unbalanced lines in DNs as well as the imperfect communication.

The voltage regulation problem is essentially an optimal power flow (OPF) problem. Conventionally, it is solved in a centralized manner assuming the availability of network-wide information [7]–[9]. Nonetheless, the centralized framework is not applicable for the real-time voltage control due to high dependence on complex communication and computation and considerable intermittence of PV generation. In this regard, a particular attention [10]–[19] has been devoted to the distributed control schemes that are more scalable and reliable as they only require neighborhood communication. Ref. [10] summarizes the recent development in the distributed and decentralized voltage control practices. Nevertheless, the previous research has rarely investigated the impact of three-phase unbalanced operation and communication delays on the distributed online voltage control.

Most existing distributed voltage control algorithms [12]–[18] are mainly designed for three-phase balanced DNs. For instance, in [12], assuming the DN is three-phase balanced, the OPF problem is formulated as a second-order cone programming (SOCP) for which a distributed algorithm is developed. In [13], a distributed adaptive robust VAR control approach is proposed to coordinate different control devices using the single-phase representation of the DN. However, in practice, DNs are inherently unbalanced due to the unequal loads on each phase and the untransposed distribution lines [20]. In [21], the proposed linearized multiphase distribution flow (LinDistFlow) model is proven to be a good approximation that accounts for the coupling effect between different phases. Recently, the multiphase LinDistFlow model has been adopted in voltage regulation problem [22]–[24]. For example, in [22], a local voltage control strategy is applied to an unbalanced DN where the power flow solution is procured using the multiphase LinDistFlow model. Nonetheless, this strategy is unable to achieve the network-wide optimal solution due to the lack of coordination between different controllers. In [23], a distributed control scheme is proposed to minimize the voltage deviations in unbalanced DNs. Similarly, the authors in [24] develop a hierarchical distributed OPF algorithm for multiphase DN. Nevertheless, all these algorithms need to solve optimization subproblems iteratively and apply the control commands after convergence. Consequently, they cannot be leveraged directly in online implementations, given the fast variations of system operating conditions.

Some research has been conducted to facilitate the effective online implementation of voltage control. The authors in [19] introduce a distributed feedback control scheme that enables instant voltage regulation. Nevertheless, it only focuses on minimizing the voltage deviations and overlooks the fact that adjusting the reactive power of PV inverters has a dramatic impact on the network power loss. Ref. [17] also proposes a feedback reactive power control design to achieve the loss minimization and voltage regulation. In our previous work [18], a distributed online voltage control algorithm is presented considering PV curtailment. However, similar to the most existing algorithms, these designs are built on three-phase balanced DNs and thus have limited applicability. In [25], to regulate the voltage profile in AC microgrids, a droop-free distributed cooperative control strategy is proposed by incorporating local measurements, while it relies on synchronous communication.

Coping with communication asynchrony is another challenge in distributed voltage control, which has not been considered in most existing works. Although a freezing strategy is proposed in [19] to overcome the communication link failures, it still requires a global timer to synchronize the updates in control variables at different buses. An asynchronous distributed OPF algorithm is proposed in [26]. While the proposed algorithm captures the stochastic communication delays, it has limited capability for online implementation and is designed for balanced DNs only. The same challenge has been tackled in other research fields, such as energy management [27], wide-area oscillation monitoring [28] and security-constrained OPF [29]. In particular, the proposed asynchronous distributed optimization approach in [30] allows local updates to be triggered by local timers only. Motivated by these, an asynchronous distributed online voltage control algorithm is proposed in this work to overcome the communication asynchrony.

Most existing distributed voltage control approaches are designed for three-phase balanced DNs only and could not cater for the online implementations. Besides, most existing voltage control algorithms are synchronous without considering the communication delays. This paper addresses these shortcomings by extending our previous work [18] on distributed online voltage control in single-phase DNs to the multiphase unbalanced DNs and developing an asynchronous updating algorithm. Specifically, we first formulate the voltage control problem as a convex quadratic programming problem. The objective is to minimize the network loss and to maintain the nodal voltages within the feasible ranges using the multiphase LinDistFlow model. Later, dual ascent method is employed to develop a synchronous distributed algorithm for solving the above problem. Finally, the synchronous algorithm is upgraded to an asynchronous one to address the communication delays. The contributions of this paper are summarized below:

- Unlike most existing distributed voltage control algorithms that are tailored for simplified single-phase representation of DNs, our proposed algorithms are intended for multiphase unbalanced DNs which are more common in practice. Moreover, the proposed algorithms incorporate the most up-to-date information collected through feedback control. This enables the algorithms to handle the fast-varying system operating conditions in online implementations; whereas, most existing works fail to adapt for such applications.
- To address the issue of communication delays which has been rarely investigated previously, we propose an asynchronous distributed voltage control algorithm inspired by [30]. The proposed algorithm allows the updates of control variables at different agents to be triggered by their local timers only. The convergence and the optimality-

guarantee of the proposed algorithms are established analytically and numerically.
- We derive the closed-form solutions to the optimization subproblems to significantly improve the computational efficiency. In addition, the communication complexity is reduced substantially to the extent that only neighborhood communication is required.
- The numerical results corroborate that our proposed algorithms outperform the benchmark approaches in terms of loss minimization and voltage regulation. Besides, the case studies validate that the proposed algorithms can eliminate voltage violations efficiently and attain the near global minimum of the network loss rapidly under the fast variation of system operating conditions.

The remainder of this paper is organized as follows. Section II introduces the system model and problem formulation. In Section III, both the synchronous and asynchronous distributed algorithms are developed. Numerical results are demonstrated in Section IV. Finally, Section V concludes the paper.

II. System Model and Problem Formulation

In this section, the voltage control problem for multiphase unbalanced DNs is formulated as a quadratic programming problem. In particular, the linearized multiphase DistFlow model is adopted and converted to a linear equation between the squared nodal voltage magnitudes and the nodal power injections. Furthermore, the network power loss is formulated as a quadratic function of nodal power injections.

A. Modelling of Multi-phase Distribution Network

Consider a DN which is typically radial. Let $\mathcal{G} = (\mathcal{N},\ \mathcal{E})$ represent the topology of the DN, where $\mathcal{N} := \{0, 1, \ldots, N\}$ and $\mathcal{E}$ represent the bus set and line set, respectively. Each bus i except the substation bus (indexed as 0) is directly connected to a unique parent bus π_i and perhaps a set of child buses, denoted by C_i. Without loss of generality, the buses are labeled in a way that the index of each bus is always greater than that of its parent bus. Besides, the line pointing from bus π_i to bus i is labeled as line i and thus $\mathcal{E} := \{1, \ldots, N\}$. Let $\mathbf{A}^0 \in \mathbb{R}^{N\times(N+1)}$ denote the line-bus incidence matrix. Hence, $A^0_{ij} = 1$ if $j = \pi_i$ and $A^0_{ij} = -1$ if $j = i$; otherwise $A^0_{ij} = 0$. Partition $\mathbf{A}^0$ into two parts as $[\mathbf{a}_0\ \mathbf{A}]$, where $\mathbf{a}_0$ denotes the first column of $\mathbf{A}^0$ which is associated with bus 0. Since $\mathcal{G}$ is a connected tree, $\mathbf{A}$ is invertible.

Without loss of generality, it is assumed that each bus in the multiphase unbalanced DN has all three phases. Then, each system variable associated with each bus or line is represented by a 3-dimensional vector. For instance, complex vector $\mathbf{V}_i := [V_i^a\ V_i^b\ V_i^c]^\top$ denotes three-phase voltages of bus i; $\mathbf{I}_i := [I_i^a\ I_i^b\ I_i^c]^\top$ and $\mathbf{S}_i := [S_i^a\ S_i^b\ S_i^c]^\top$ denote the line current and power flow on line i, respectively. Different phases are coupled with each other through Ohm's law:

$$\mathbf{V}_i = \mathbf{V}_{\pi_i} - \mathbf{z}_i\mathbf{I}_i \tag{1}$$

where $\mathbf{z}_i := \mathbf{r}_i + j\mathbf{x}_i \in \mathbb{C}^{3\times3}$ denotes the impedance matrix of line i, which is a 3×3 full symmetric complex matrix.

In voltage regulation, only voltage magnitudes are useful. Thus, both sides of (1) are multiplied by their complex conjugates $(*)$ to eliminate voltage angles, as shown below.

$$\mathbf{v}_i = \mathbf{v}_{\pi_i} - 2\mathrm{Re}\left[\mathbf{V}_{\pi_i} \odot (\mathbf{z}_i^*\mathbf{I}_i^*)\right] + (\mathbf{z}_i\mathbf{I}_i) \odot (\mathbf{z}_i^*\mathbf{I}_i^*) \tag{2}$$

where $\mathbf{v}_i := [v_i^a\ v_i^b\ v_i^c]^\top = \mathbf{V}_i \odot \mathbf{V}_i^* \in \mathbb{R}^3$ is the vector of squared voltage magnitudes at bus i, $\odot$ denotes the element-wise product. Note that the last term on the right-hand side of (2) is relatively small due to the small entries of $\mathbf{z}_i$ and thus can be neglected. To simplify the second term on the right-hand side of (2), it is further assumed that phase voltages are approximately balanced [22]. Hence, we approximate $\mathbf{V}_i$ by $\tilde{V}_i\boldsymbol{\alpha}$, where $\tilde{V}_i$ denotes the voltage magnitude, $\boldsymbol{\alpha} := [1\ \alpha\ \alpha^2]^\top$ and $\alpha = e^{-j(2\pi/3)}$. Then, the conjugate of line current $\mathbf{I}_i^*$ can be approximated by

$$\mathbf{I}_i^* = \mathbf{S}_i \oslash \mathbf{V}_{\pi_i} \approx \frac{1}{\tilde{V}_{\pi_i}}\boldsymbol{\alpha}^* \odot \mathbf{S}_i \tag{3}$$

where $\oslash$ denotes element-wise division. Hence, $\mathbf{V}_{\pi_i} \odot (\mathbf{z}_i^*\mathbf{I}_i^*)$ can be reformulated as

$$\begin{aligned}\mathbf{V}_{\pi_i} \odot (\mathbf{z}_i^*\mathbf{I}_i^*) &= \boldsymbol{\alpha} \odot \left[\mathbf{z}_i^* \left(\boldsymbol{\alpha}^* \odot \mathbf{S}_i\right)\right] \\ &= \mathrm{diag}(\boldsymbol{\alpha})\mathbf{z}_i^*\mathrm{diag}(\boldsymbol{\alpha}^*)\mathbf{S}_i \\ &= \tilde{\mathbf{z}}_i^*\mathbf{S}_i\end{aligned} \tag{4}$$

where $\tilde{\mathbf{z}}_i := \mathrm{diag}(\boldsymbol{\alpha}^*)\mathbf{z}_i\mathrm{diag}(\boldsymbol{\alpha}) \in \mathbb{C}^{3\times3}$ is a constant matrix. The first equality follows by plugging $\mathbf{V}_i \approx \tilde{V}_i\boldsymbol{\alpha}$ and (3). The second equality holds due to the following property: $\mathbf{x} \odot \mathbf{y} = \mathrm{diag}(\mathbf{x})\mathbf{y}$. Thus, (2) is reformulated as (5) by plugging (4).

$$\mathbf{v}_{\pi_i} - \mathbf{v}_i = 2\mathrm{Re}\left(\tilde{\mathbf{z}}_i^*\mathbf{S}_i\right) \tag{5}$$

The power flow balance equation at each bus i is given by

$$\mathbf{S}_i - (\mathbf{z}_i\mathbf{I}_i) \odot \mathbf{I}_i^* - \sum_{j\in C_i}\mathbf{S}_j = -\mathbf{s}_i \tag{6}$$

where the second term on the left-hand side represents the power loss on line i, which is relatively small compared to the line flows and is neglected. The linear approximation of (6) ignoring the power loss is obtained as

$$\mathbf{S}_i - \sum_{j\in C_i}\mathbf{S}_j = -\mathbf{s}_i \tag{7}$$

Equations (5) and (7) form the linearized multiphase DistFlow model.

For mathematical conciseness, all variables associated with non-substation buses are represented by vectors as $\mathbf{s} := [\mathbf{s}_1^\top \cdots \mathbf{s}_N^\top]^\top \in \mathbb{C}^{3N}$ and $\mathbf{v} := [\mathbf{v}_1^\top \cdots \mathbf{v}_N^\top]^\top \in \mathbb{R}^{3N}$ and all variables associated with lines are shown in vectors $\mathbf{S} := [\mathbf{S}_1^\top \cdots \mathbf{S}_N^\top]^\top \in \mathbb{C}^{3N}$. Then, (5) and (7) can be written in compact form as

$$(\mathbf{A} \otimes \mathbf{I}_3)\mathbf{v} = 2\mathrm{Re}\big[\mathrm{bdiag}(\tilde{\mathbf{z}}_i^*)\mathbf{S}\big] - v_0 \cdot (\mathbf{a}_0 \otimes \mathbf{1}_3) \tag{8a}$$

$$\mathbf{S} = \mathbf{M}\mathbf{s} \tag{8b}$$

where $\mathrm{bdiag}(\cdot)$ denotes the operator to construct the block-wise diagonal matrix using a set of square matrices, $\mathbf{I}_3$ is the 3-dimensional identity matrix, $\mathbf{M} := \mathbf{A}^{-\top} \otimes \mathbf{I}_3 \in \mathbb{R}^{3N\times3N}$ and $\otimes$ denotes the Kronecker product.

Plugging (8b) into (8a), the linearized multiphase DistFlow model can be equivalently converted to the following equation.

$$\mathbf{v} = \mathbf{R}\mathbf{p} + \mathbf{X}\mathbf{q} + v_0\mathbf{1}_{3N} \tag{9}$$

where $\mathbf{R} := 2\mathbf{M}^\top \text{bdiag}\left([\text{Re}(\tilde{\mathbf{z}}_i)]\right)\mathbf{M}$ and $\mathbf{X} := 2\mathbf{M}^\top \text{bdiag}\left([\text{Im}(\tilde{\mathbf{z}}_i)]\right)\mathbf{M}$ are $3N \times 3N$ real matrices.

B. Optimization Model of VAR Control

The voltage control can be efficiently accomplished by adjusting the reactive power outputs of PV inverters, while the active power outputs are fixed at maximum power points to fully harvest the solar energy. The reactive power output of PV inverter on phase ϕ of bus i is constrained by

$$-\sqrt{S_{i,\phi}^2 - \left(p_{i,\phi}^s\right)^2} \le q_{i,\phi}^s \le \sqrt{S_{i,\phi}^2 - \left(p_{i,\phi}^s\right)^2} \tag{10}$$

where $S_{i,\phi}$ and $p_{i,\phi}^s$ are the rated apparent power of PV inverter and the instantaneous maximum available active power.

As discussed earlier, adjusting the reactive power of PV inverters has a strong impact on the network loss. Hence, it is necessary to take the network loss into consideration. The active power loss on line i, can be expressed as

$$\text{Loss}_i = \text{Re}\left[(\mathbf{V}_{\pi_i} - \mathbf{V}_i)^\top \mathbf{I}_i^*\right] = \text{Re}\left[\mathbf{I}_i^\top \mathbf{z}_i \mathbf{I}_i^*\right] \tag{11}$$

where the approximation of $\mathbf{I}_i^*$ is obtained as (3). Here, it is assumed that $\tilde{V}_{\pi_i} \approx 1,\ \forall i \in \mathcal{N}\backslash 0$. Therefore, $\mathbf{I}_i^* \approx \text{diag}(\boldsymbol{\alpha}^*)\mathbf{S}_i$. Plugging it into (11), the approximation of Loss_i is shown as

$$\begin{aligned}\text{Loss}_i &\approx \text{Re}\left[\mathbf{S}_i^H \text{diag}(\boldsymbol{\alpha})\mathbf{z}_i \text{diag}(\boldsymbol{\alpha}^*)\mathbf{S}_i\right] \\ &= \mathbf{S}_i^H \text{diag}(\boldsymbol{\alpha})\mathbf{r}_i \text{diag}(\boldsymbol{\alpha}^*)\mathbf{S}_i \\ &= \mathbf{S}_i^H \tilde{\mathbf{r}}_i \mathbf{S}_i\end{aligned} \tag{12}$$

where $\tilde{\mathbf{r}}_i := \text{diag}(\boldsymbol{\alpha})\mathbf{r}_i\text{diag}(\boldsymbol{\alpha}^*) \in \mathbb{C}^{3\times 3}$, and $\mathbf{S}_i^H$ is the complex Hermitian of $\mathbf{S}_i$. Hence, the total active power loss can be obtained by summing up all line losses as

$$\begin{aligned}\text{Loss} &= \mathbf{S}^H \tilde{\mathbf{r}} \mathbf{S} \\ &= \mathbf{s}^H \mathbf{M}^\top \tilde{\mathbf{r}} \mathbf{M} \mathbf{s} \\ &= \mathbf{p}^\top \tilde{\mathbf{R}}_r \mathbf{p} + \mathbf{q}^\top \tilde{\mathbf{R}}_r \mathbf{q} + 2\mathbf{q}^\top \tilde{\mathbf{R}}_x \mathbf{p}\end{aligned} \tag{13}$$

where $\tilde{\mathbf{r}} := \text{bdiag}(\tilde{\mathbf{r}}_i) \in \mathbb{C}^{3N\times 3N}$, $\tilde{\mathbf{R}}_r := \mathbf{M}^\top \text{Re}(\tilde{\mathbf{r}})\mathbf{M} \in \mathbb{R}^{3N\times 3N}$ and $\tilde{\mathbf{R}}_x := \mathbf{M}^\top \text{Im}(\tilde{\mathbf{r}})\mathbf{M} \in \mathbb{R}^{3N\times 3N}$. The second equality follows by plugging (8b) and the third equality follows by expanding $\mathbf{M}^\top\tilde{\mathbf{r}}\mathbf{M}$ and $\mathbf{s}$. Eq. (13) shows the total power loss is a quadratic function of nodal power injections.

Therefore, the VAR control problem for the multiphase unbalanced DN can be formulated as

$$\min_{\mathbf{q}} \ \mathbf{q}^\top \tilde{\mathbf{R}}_r \mathbf{q} + 2\mathbf{q}^\top \tilde{\mathbf{R}}_x \mathbf{p} \tag{14a}$$

$$\text{s.t. } \mathbf{v} = \mathbf{R}\mathbf{p} + \mathbf{X}\mathbf{q} + v_0\mathbf{1}_{3N} \tag{14b}$$

$$\underline{\mathbf{v}} \le \mathbf{v} \le \overline{\mathbf{v}} \tag{14c}$$

$$\underline{\mathbf{q}} \le \mathbf{q} \le \overline{\mathbf{q}} \tag{14d}$$

where the objective is to minimize the total network loss. Since only the reactive power is controllable, the term $\mathbf{p}^\top \tilde{\mathbf{R}}_r \mathbf{p}$ is a constant and thus dropped. Constraint (14c) is to ensure the bus voltages are within the acceptable ranges and (14d) imposes limits on the nodal reactive power injections. Specifically, $\underline{q}_{i,\phi} = \overline{q}_{i,\phi} = -q_{i,\phi}^l$ if node (i,ϕ) has no PV installation, where $q_{i,\phi}^l$ denotes the reactive load at node (i,ϕ). If node (i,ϕ) has PV installation, $\underline{q}_{i,\phi} = -q_{i,\phi}^l - \sqrt{S_{i,\phi}^2 - \left(p_{i,\phi}^s\right)^2}$ and $\overline{q}_{i,\phi} = -q_{i,\phi}^l + \sqrt{S_{i,\phi}^2 - \left(p_{i,\phi}^s\right)^2}$. Here, each node represents one phase of a bus.

III. Distributed Online VAR Control Algorithm

In this section, first, a synchronous distributed algorithm is developed for solving the problem (14) and the online implementation is facilitated by incorporating the feedback control. In particular, the closed-form solutions are derived for updating the control variables, and the communication requirement is simplified to the extent that only neighborhood information exchange is required. Later, an asynchronous distributed algorithm is presented to overcome the communication asynchrony.

A. Sychronous Distributed Algorithm

The proposed algorithm is developed by using the dual ascent method and the core idea is to iteratively update the primal and dual variables [31]. In the synchronous paradigm, all agents simultaneously update their local control variables at each iteration. The Lagrangian function of problem (14) is formulated as

$$\begin{aligned}\mathcal{L} =& \mathbf{q}^\top \tilde{\mathbf{R}}_r \mathbf{q} + 2\mathbf{q}^\top \tilde{\mathbf{R}}_x \mathbf{p} + \underline{\boldsymbol{\mu}}^\top (\underline{\mathbf{v}} - \mathbf{R}\mathbf{p} - \mathbf{X}\mathbf{q} \\ &- v_0\mathbf{1}_{3N}) + \overline{\boldsymbol{\mu}}^\top (\mathbf{R}\mathbf{p} + \mathbf{X}\mathbf{q} + v_0\mathbf{1}_{3N} - \overline{\mathbf{v}}) \\ &+ \underline{\boldsymbol{\omega}}^\top (\underline{\mathbf{q}} - \mathbf{q}) + \overline{\boldsymbol{\omega}}^\top (\mathbf{q} - \overline{\mathbf{q}})\end{aligned} \tag{15}$$

where $\underline{\boldsymbol{\mu}} := [\underline{\boldsymbol{\mu}}_1^\top, \cdots, \underline{\boldsymbol{\mu}}_N^\top]^\top$, $\overline{\boldsymbol{\mu}} := [\overline{\boldsymbol{\mu}}_1^\top, \cdots, \overline{\boldsymbol{\mu}}_N^\top]^\top$, $\underline{\boldsymbol{\omega}} := [\underline{\boldsymbol{\omega}}_1^\top, \cdots, \underline{\boldsymbol{\omega}}_N^\top]^\top$ and $\overline{\boldsymbol{\omega}} := [\overline{\boldsymbol{\omega}}_1^\top, \cdots, \overline{\boldsymbol{\omega}}_N^\top]^\top$ are Lagrangian multipliers (dual variables) related to (14c) and (14d), respectively. $\underline{\boldsymbol{\mu}}_i, \overline{\boldsymbol{\mu}}_i, \underline{\boldsymbol{\omega}}_i$ and $\overline{\boldsymbol{\omega}}_i$ are 3-dimensional vectors associated with bus i.

1) Update of dual variables: Using gradient projection method, each bus i can locally update its dual variables at each iteration using (16) with no communication.

$$\underline{\boldsymbol{\mu}}_i^{(k+1)} = \left[\underline{\boldsymbol{\mu}}_i^{(k)} + \underline{\alpha}_i(\underline{\mathbf{v}}_i - \mathbf{v}_i^{(k)})\right]^+ \tag{16a}$$

$$\overline{\boldsymbol{\mu}}_i^{(k+1)} = \left[\overline{\boldsymbol{\mu}}_i^{(k)} + \overline{\alpha}_i(\mathbf{v}_i^{(k)} - \overline{\mathbf{v}}_i)\right]^+ \tag{16b}$$

$$\underline{\boldsymbol{\omega}}_i^{(k+1)} = \left[\underline{\boldsymbol{\omega}}_i^{(k)} + \underline{\gamma}_i(\underline{\mathbf{q}}_i - \mathbf{q}_i^{(k)})\right]^+ \tag{16c}$$

$$\overline{\boldsymbol{\omega}}_i^{(k+1)} = \left[\overline{\boldsymbol{\omega}}_i^{(k)} + \overline{\gamma}_i(\mathbf{q}_i^{(k)} - \overline{\mathbf{q}}_i)\right]^+ \tag{16d}$$

where $\underline{\alpha}_i,\ \overline{\alpha}_i,\ \underline{\gamma}_i$ and $\overline{\gamma}_i$ are the step sizes, and $[\cdot]^+$ denotes the projection operator onto the non-negative range.

2) Update of primal variables: For mathematical conciseness, we omit the iteration index k in the following unless otherwise specified. Since $\mathcal{L}$ is a quadratic function of $\mathbf{q}$, a closed-form solution of $\mathbf{q}$ that minimizes $\mathcal{L}$ can be calculated as

$$\mathbf{q} = \frac{1}{2}\tilde{\mathbf{R}}_r^{-1}\left(-2\tilde{\mathbf{R}}_x\mathbf{p} + \mathbf{X}^\top\underline{\boldsymbol{\mu}} - \mathbf{X}^\top\overline{\boldsymbol{\mu}} + \underline{\boldsymbol{\omega}} - \overline{\boldsymbol{\omega}}\right) \tag{17}$$

By exploiting the closed-form solution, the computation cost is significantly reduced as it only involves trivial algebraic operations. The communication complexity is also minimized such that each bus only needs to exchange partial information with its neighbors to update the primal variable $\mathbf{q}_i$. To demonstrate the communication simplicity, two important Propositions are provided and the updating formula for $\mathbf{q}_i$ at each bus i is explicitly derived.

Proposition 1. *Let* $\mathbf{B}$ *denote the inverse of* $\tilde{\mathbf{R}}_r$*, i.e.,* $\mathbf{B} := \tilde{\mathbf{R}}_r^{-1}$*. We partition* $\mathbf{B}$ *into* $N \times N$ *blocks with each block being a* 3×3 *square matrix. Then, for any pair of buses* (i, j) *that are not directly connected, the corresponding submatrix* $\mathbf{B}_{ij}$ *is a* 3×3 *zero matrix.*

Proof. By definition of $\tilde{\mathbf{R}}_r$, we have

$$\begin{aligned}\tilde{\mathbf{R}}_r^{-1} &= (\mathbf{A}^\top \otimes \mathbf{I}_3)\text{bdiag}\big[\text{Re}(\tilde{\mathbf{r}}_i)^{-1}\big](\mathbf{A} \otimes \mathbf{I}_3)\\ &= \mathbf{U}\text{bdiag}\big[\text{Re}(\tilde{\mathbf{r}}_i)^{-1}\big]\mathbf{U}^\top\end{aligned}$$

where $\mathbf{U} := \mathbf{A}^\top \otimes \mathbf{I}_3$. The same partition is applied to matrix $\mathbf{U}$ and therefore $\mathbf{U}_{ik} = A_{ki}\mathbf{I}_3$ and $\mathbf{U}_{jk} = A_{kj}\mathbf{I}_3$. Using the block matrix multiplication rule, the submatrix $\mathbf{B}_{ij}$ can be calculated by

$$\mathbf{B}_{ij} = \sum_{k=1}^{N} \mathbf{U}_{ik}\text{Re}(\tilde{\mathbf{r}}_k)^{-1}\mathbf{U}_{jk} = \sum_{k=1}^{N} A_{ki}A_{kj}\text{Re}(\tilde{\mathbf{r}}_k)^{-1} \tag{18}$$

Then, if $j \neq i$ and bus j is not directly connected to bus i, $A_{ki}A_{kj} = 0, \forall k \in \mathcal{E}$ according to the definition of $\mathbf{A}$. Subsequently, $\mathbf{B}_{ij}$ is a 3×3 zero matrix. □

Proposition 2. *Let* $\boldsymbol{\beta} := [\boldsymbol{\beta}_1^\top \cdots \boldsymbol{\beta}_N^\top]^\top \in \mathbb{R}^{3N}$ *denote* $\tilde{\mathbf{R}}_r^{-1}\tilde{\mathbf{R}}_x\mathbf{p}$*, where each* $\boldsymbol{\beta}_i$ *is a 3-dimensional vector associated with bus* i*. Then, the update of* $\boldsymbol{\beta}_i$ *only involves information exchange between bus* i *and its set of child buses* C_i*.*

Proof. Plugging $\tilde{\mathbf{R}}_r := \mathbf{M}^\top\text{Re}(\tilde{\mathbf{r}})\mathbf{M}$ and $\tilde{\mathbf{R}}_x := \mathbf{M}^\top\text{Im}(\tilde{\mathbf{r}})\mathbf{M}$ into $\tilde{\mathbf{R}}_r^{-1}\tilde{\mathbf{R}}_x\mathbf{p}$, we have

$$\begin{aligned}\tilde{\mathbf{R}}_r^{-1}\tilde{\mathbf{R}}_x\mathbf{p} =& \mathbf{M}^{-1}\text{bdiag}\big[\text{Re}(\tilde{\mathbf{r}}_i)^{-1}\text{Im}(\tilde{\mathbf{r}}_i)\big]\mathbf{M}\mathbf{p}\\ =& \mathbf{M}^{-1}\text{bdiag}\big[\text{Re}(\tilde{\mathbf{r}}_i)^{-1}\text{Im}(\tilde{\mathbf{r}}_i)\big]\mathbf{P}\\ =& (\mathbf{A}^\top \otimes \mathbf{I}_3)\tilde{\mathbf{P}}\end{aligned} \tag{19}$$

where $\mathbf{P} = [\mathbf{P}_1^\top \cdots \mathbf{P}_N^\top]^\top$ is the vector of active line flows and $\mathbf{P}_i \in \mathbb{R}^3$ is the three-phase active power flow on line i (from bus π_i to bus i); $\tilde{\mathbf{P}} := [\tilde{\mathbf{P}}_1^\top \cdots \tilde{\mathbf{P}}_N^\top]^\top$ and $\tilde{\mathbf{P}}_i = \text{Re}(\tilde{\mathbf{r}}_i)^{-1}\text{Im}(\tilde{\mathbf{r}}_i)\mathbf{P}_i$. The second equality in (19) holds due to $\mathbf{P} = \mathbf{M}\mathbf{p}$ and the last equality follows by plugging $\mathbf{M}$. Thus, for each $\boldsymbol{\beta}_i$, we have

$$\boldsymbol{\beta}_i = \sum_{j=1}^{N} A_{ji}\tilde{\mathbf{P}}_j = -\tilde{\mathbf{P}}_i + \sum_{j\in C_i} \tilde{\mathbf{P}}_j \tag{20}$$

where the second equality in (20) is derived using the definition of matrix $\mathbf{A}$. Therefore, each bus i only needs its own information, i.e., $\tilde{\mathbf{P}}_i$, and partial information from its child buses, i.e., $\tilde{\mathbf{P}}_j$, $j \in C_i$, to update $\boldsymbol{\beta}_i$. □

Next, the second and third terms on the right hand side of the expanded form of (17) are simplified to the extent that only local information is required for the update at each bus. Let $\underline{\boldsymbol{\zeta}} := [\underline{\boldsymbol{\zeta}}_1^\top \cdots \underline{\boldsymbol{\zeta}}_N^\top]^\top \in \mathbb{R}^{3N}$ and $\overline{\boldsymbol{\zeta}} := [\overline{\boldsymbol{\zeta}}_1^\top \cdots \overline{\boldsymbol{\zeta}}_N^\top]^\top \in \mathbb{R}^{3N}$ denote $\frac{1}{2}\tilde{\mathbf{R}}_r^{-1}\mathbf{X}^\top\underline{\boldsymbol{\mu}}$ and $\frac{1}{2}\tilde{\mathbf{R}}_r^{-1}\mathbf{X}^\top\overline{\boldsymbol{\mu}}$, respectively, where $\underline{\boldsymbol{\zeta}}_i$ and $\overline{\boldsymbol{\zeta}}_i$ are 3-dimensional vectors associated with bus i. For conciseness, only the update of $\underline{\boldsymbol{\zeta}}_i$ is illustrated as the update of $\overline{\boldsymbol{\zeta}}_i$ can be derived accordingly. Plugging $\tilde{\mathbf{R}}_r := \mathbf{M}^\top\text{bdiag}[\text{Re}(\tilde{\mathbf{r}}_i)]\mathbf{M}$ and $\mathbf{X} := 2\mathbf{M}^\top\text{bdiag}\left([\text{Im}(\tilde{\mathbf{z}}_i)]\right)\mathbf{M}$ into $\frac{1}{2}\tilde{\mathbf{R}}_r^{-1}\mathbf{X}^\top\underline{\boldsymbol{\mu}}$, we have

$$\begin{aligned}\frac{1}{2}\tilde{\mathbf{R}}_r^{-1}\mathbf{X}^\top\underline{\boldsymbol{\mu}} =& \mathbf{M}^{-1}\text{bdiag}\big[\text{Re}(\tilde{\mathbf{r}}_i)^{-1}\text{Im}(\tilde{\mathbf{z}}_i)^\top\big]\mathbf{M}\underline{\boldsymbol{\mu}}\\ =& \mathbf{M}^{-1}\text{bdiag}\big[\text{Re}(\tilde{\mathbf{r}}_i)^{-1}\text{Im}(\tilde{\mathbf{z}}_i)^\top\big]\underline{\boldsymbol{\lambda}}\\ =& (\mathbf{A}^\top \otimes \mathbf{I}_3)\underline{\boldsymbol{\xi}}\end{aligned} \tag{21}$$

where $\underline{\boldsymbol{\lambda}} := [\underline{\boldsymbol{\lambda}}_1^\top \cdots \underline{\boldsymbol{\lambda}}_N^\top]^\top := \mathbf{M}\underline{\boldsymbol{\mu}}$ and each $\underline{\boldsymbol{\lambda}}_i$ is a 3-dimensional vector associated with the corresponding bus i; $\underline{\boldsymbol{\xi}} := [\underline{\boldsymbol{\xi}}_1^\top, \cdots, \underline{\boldsymbol{\xi}}_N^\top]^\top$ and $\underline{\boldsymbol{\xi}}_i := \text{Re}(\tilde{\mathbf{r}}_i)^{-1}\text{Im}(\tilde{\mathbf{z}}_i)^\top\underline{\boldsymbol{\lambda}}_i \in \mathbb{R}^3$. By observing (7) and (8b), we have

$$\underline{\boldsymbol{\lambda}}_i = \sum_{j\in C_i} \underline{\boldsymbol{\lambda}}_j - \underline{\boldsymbol{\mu}}_i \tag{22}$$

Like (20), $\underline{\boldsymbol{\zeta}}_i$ can be expressed as

$$\underline{\boldsymbol{\zeta}}_i = \sum_{j=1}^{N} A_{ji}\underline{\boldsymbol{\xi}}_j = -\underline{\boldsymbol{\xi}}_i + \sum_{j\in C_i} \underline{\boldsymbol{\xi}}_j \tag{23}$$

Let K_i denote $\text{Re}(\tilde{\mathbf{r}}_i)^{-1}\text{Im}(\tilde{\mathbf{z}}_i)^\top$. Substituting $\underline{\boldsymbol{\xi}}_i := K_i\underline{\boldsymbol{\lambda}}_i$ and (22) into (23), we have

$$\underline{\boldsymbol{\zeta}}_i = K_i\underline{\boldsymbol{\mu}}_i + \sum_{j\in C_i} (K_j - K_i)\underline{\boldsymbol{\lambda}}_j \tag{24}$$

Note that for a large portion of buses in a distribution system, the line connecting a bus to its parent bus (incoming line) is homogeneous with the lines connecting it to its child buses (outgoing lines). Thus, $K_i = K_j, \forall j \in C_i$, which gives rise to $\underline{\boldsymbol{\zeta}}_i = K_i\underline{\boldsymbol{\mu}}_i$. For buses whose incoming line is heterogeneous with the outgoing lines, K_i is unequal to K_j for some $j \in C_i$. However, due to $\|K_j - K_i\| \ll \|K_i\|$, the term $\sum_{j\in C_i}(K_j - K_i)\underline{\boldsymbol{\lambda}}_j$ can still be neglected for these buses as it is relatively small compared with other terms. Therefore, the entries of $\frac{1}{2}\tilde{\mathbf{R}}_r^{-1}\mathbf{X}^\top\underline{\boldsymbol{\mu}}$ and $\frac{1}{2}\tilde{\mathbf{R}}_r^{-1}\mathbf{X}^\top\overline{\boldsymbol{\mu}}$ associated with bus i are expressed as

$$\underline{\boldsymbol{\zeta}}_i \approx K_i\underline{\boldsymbol{\mu}}_i \tag{25a}$$

$$\overline{\boldsymbol{\zeta}}_i \approx K_i\overline{\boldsymbol{\mu}}_i \tag{25b}$$

With Propositions 1 and 2 as well as (25), the explicit update formula for primal variables at each bus i is derived as

$$\tilde{\mathbf{q}}_i \approx \tilde{\mathbf{P}}_i - \sum_{j\in C_i} \tilde{\mathbf{P}}_j + K_i(\underline{\boldsymbol{\mu}}_i - \overline{\boldsymbol{\mu}}_i) + \sum_{j\in\{i,\pi_i,C_i\}} \frac{1}{2}\mathbf{B}_{ij}(\underline{\boldsymbol{\omega}}_j - \overline{\boldsymbol{\omega}}_j) \tag{26}$$

where $\tilde{\mathbf{q}}_i$ is the approximation of $\mathbf{q}_i$. It can observed that bus i only needs to know its own information and partial information of its neighbors, i.e., the parent bus π_i and child buses C_i, to update the primal variables.

Due to the relaxation of constraint (14d), the primal variables calculated from (26) might be infeasible. Hence, the reactive power injection on each node (ϕ, i) should be projected onto its feasible range as

$$q_{i,\phi}^{\text{act}} = \left[\tilde{q}_{i,\phi}\right]_{\underline{q}_{i,\phi}}^{\overline{q}_{i,\phi}} \tag{27}$$

where $[\cdot]_a^b$ denotes the projection operator onto the range $[a, b]$.

3) Online Implementation: The proposed distributed algorithm leverages the feedback control to enable online implementation. Here, each bus only needs minimal communication and computation overhead to update the local control variables. Each iteration of the algorithm consists of the following five steps:

Step 1: Measure the local voltage magnitude and real power flow on the incoming line at bus i.

Step 2: Calculate $\tilde{\mathbf{P}}_i$ and update dual variables using (16).

Step 3: Send $\tilde{\mathbf{P}}_i$ to the parent bus and $\underline{\boldsymbol{\omega}}_i, \overline{\boldsymbol{\omega}}_i$ to the neighboring buses. Meanwhile, receive $\tilde{\mathbf{P}}_j$ from the child buses and $\underline{\boldsymbol{\omega}}_j, \overline{\boldsymbol{\omega}}_j$ from the neighboring buses.

Step 4: Update primal variables using (26) and project $\tilde{\mathbf{q}}_i$ onto the feasible region as (27).

Step 5: Apply the reactive power set points at each bus.

B. Convergence Analysis

Lemma 1. *Problem (14) is strictly convex.*

Proof. To substantiate strict convexity, it suffices to show the matrix $\tilde{\mathbf{R}}_r$ is positive definite. Since the resistance matrix $\mathbf{r}_i$ is symmetric and $\alpha^2 = \alpha^* = -\frac{1}{2} + j\frac{\sqrt{3}}{2}$, we have

$$\text{Re}(\tilde{\mathbf{r}}_i) = \frac{1}{2}\begin{bmatrix} 2r_i^{aa} & -r_i^{ab} & -r_i^{ac} \\ -r_i^{ab} & 2r_i^{bb} & -r_i^{bc} \\ -r_i^{ac} & -r_i^{bc} & 2r_i^{cc} \end{bmatrix} \tag{28}$$

where $r_i^{\phi_1\phi_1}$ is the self-resistance of phase ϕ_1 and $r_i^{\phi_1\phi_2}$ is the mutual-resistance between phase ϕ_1 and phase ϕ_2. We can see the matrix $\text{Re}(\tilde{\mathbf{r}}_i)$ is symmetric. Moreover, it is positive definite because it is strictly diagonally dominant. Hence, the matrix $\tilde{\mathbf{R}}_r := \mathbf{M}^\top \text{bdiag}[\text{Re}(\tilde{\mathbf{r}}_i)]\mathbf{M}$ is also positive definite. Therefore, problem (14) is strictly convex. □

For mathematical conciseness, problem (14) is further rewritten as the following problem.

$$\min_{\mathbf{x}} \ \frac{1}{2}\mathbf{x}^\top \mathbf{H}\mathbf{x} + \mathbf{c}^\top \mathbf{x} \tag{29a}$$

$$\text{s.t. } \mathbf{E}\mathbf{x} \le \mathbf{b} \tag{29b}$$

where $\mathbf{x}$ collects the decision variables of (14); $\mathbf{H}$ and $\mathbf{c}$ are the coefficient matrix and vector of the quadratic and linear terms in the objective function, respectively. $\mathbf{E}$ and $\mathbf{b}$ are the coefficient matrix and vector of the linear constraints, respectively. Since problem (29) is strictly convex, its dual problem can be derived as

$$\max_{\mathbf{y}\ge 0} g(\mathbf{y}) = -\frac{1}{2}\mathbf{y}^\top \mathbf{E}\mathbf{H}^{-1}\mathbf{E}^\top \mathbf{y} - (\mathbf{E}\mathbf{H}^{-1}\mathbf{c} + \mathbf{b})^\top \mathbf{y} - \frac{1}{2}\mathbf{c}^\top \mathbf{H}^{-1}\mathbf{c} \tag{30}$$

where $\mathbf{y}$ is the dual variable collecting $\underline{\boldsymbol{\mu}}, \overline{\boldsymbol{\mu}}, \underline{\boldsymbol{\omega}}$ and $\overline{\boldsymbol{\omega}}$.

Theorem 1. *Given the dual and primal updating formulas (16) and (26), the updating direction vector of the dual variables is a close approximation of the gradient of the dual function, i.e., ∇g. Then, the trajectories of primal variables ($\mathbf{q}$) and dual variables ($\underline{\boldsymbol{\mu}}, \overline{\boldsymbol{\mu}}, \underline{\boldsymbol{\omega}}, \overline{\boldsymbol{\omega}}$) asymptotically converge to the optimal primal and dual solutions, respectively, if the step sizes are selected in a way such that the largest eigenvalue of the matrix $\mathbf{D}^{\frac{1}{2}}\mathbf{E}\mathbf{H}\mathbf{E}^\top\mathbf{D}^{\frac{1}{2}}$ is smaller than 2, where $\mathbf{D}$ is the diagonal matrix of step sizes.*

Proof. As we illustrated in our previous work [18], if the iterations of primal and dual variables follow the exact updating formulas (16) and (17), the updating direction of the dual variable is the gradient of the dual function, i.e., $\nabla g = [(\underline{\mathbf{v}} - \mathbf{v})^\top, (\mathbf{v} - \overline{\mathbf{v}})^\top, (\underline{\mathbf{q}} - \mathbf{q})^\top, (\mathbf{q} - \overline{\mathbf{q}})^\top]^\top$. Furthermore, the convergence is guaranteed if the step sizes meet the condition that the largest eigenvalue of the matrix $\mathbf{D}^{\frac{1}{2}}\mathbf{E}\mathbf{H}\mathbf{E}^\top\mathbf{D}^{\frac{1}{2}}$ is smaller than 2 [31]. Hence, to establish the convergence of the proposed synchronous distributed algorithm, it suffices to show that the updating direction of the dual variables Δy using approximated updating formulas (16) and (26), is a close approximation of the gradient ∇g. To this end, let $\Delta\mathbf{q}_i$ denote the neglected item in the approximated primal update formula, i.e., $\tilde{\mathbf{q}}_i = \mathbf{q}_i - \Delta\mathbf{q}_i$. Then, Δy can be expressed as

$$\Delta y = \begin{bmatrix} \underline{\mathbf{v}} - \tilde{\mathbf{v}} \\ \tilde{\mathbf{v}} - \overline{\mathbf{v}} \\ \underline{\mathbf{q}} - \tilde{\mathbf{q}} \\ \tilde{\mathbf{q}} - \overline{\mathbf{q}} \end{bmatrix} = \begin{bmatrix} \underline{\mathbf{v}} - \mathbf{v} + \mathbf{X}\Delta\mathbf{q} \\ \mathbf{v} - \overline{\mathbf{v}} - \mathbf{X}\Delta\mathbf{q} \\ \underline{\mathbf{q}} - \mathbf{q} + \Delta\mathbf{q} \\ \mathbf{q} - \overline{\mathbf{q}} - \Delta\mathbf{q} \end{bmatrix} = \nabla g + \delta g \tag{31}$$

where $\delta g := [(\mathbf{X}\Delta\mathbf{q})^\top, -(\mathbf{X}\Delta\mathbf{q})^\top, (\Delta\mathbf{q})^\top, -(\Delta\mathbf{q})^\top]^\top$. Indeed, Δy is a good approximation of ∇g as δg is negligibly small due to the following features of DNs. Firstly, a large portion of buses in DNs have homogeneous incoming and outgoing lines, which means for most buses $\tilde{\mathbf{q}}_i = \mathbf{q}_i$ and hence $\Delta\mathbf{q}_i = 0$. Secondly, for buses with heterogeneous incoming and outgoing lines the inequality $\|K_j - K_i\| \ll \|K_i\|$ holds. Thus, the neglected items $\sum_{j\in C_i}(K_j - K_i)\underline{\boldsymbol{\lambda}}_j$ are relatively small compared with $\tilde{\mathbf{q}}_i$. The third one is that the entries of the matrix $\mathbf{X}$ are comparatively small, and hence the entries of $\mathbf{X}\Delta\mathbf{q}$ are high-order small terms. Finally, for most buses $\underline{\mathbf{v}}_i < \mathbf{v}_i < \overline{\mathbf{v}}_i$ and $\underline{\mathbf{q}}_i < \mathbf{q}_i < \overline{\mathbf{q}}_i$, and hence $\|\nabla g\| \gg \|\delta g\|$. Therefore, Δy is a good approximation of the gradient ∇g and hence the convergence property in [18] also applies to the proposed synchronous algorithm. □

C. Asynchronous Distributed Algorithm

In contrast to the synchronous algorithm, the updates of control variables at different agents/buses are only triggered by their local timers instead of a global clock. Fig. 1 shows an example of the updating timelines of two agents using the asynchronous algorithm. Here, each agent has its own duty cycle consists of two states, namely the idle state and the awake state. The duration of the awake state is negligibly short because of the computation and communication simplicity.

Algorithm 1 summarizes the asynchronous distributed algorithm for online voltage control. Each agent makes decisions

Algorithm 1: Asynchronous Distributed Algorithm for Online Voltage Control

Decision variables: $\tilde{\mathbf{q}}_i, \underline{\boldsymbol{\mu}}_i, \overline{\boldsymbol{\mu}}_i, \underline{\boldsymbol{\omega}}_i, \overline{\boldsymbol{\omega}}_i$

Initialization: set $\tau_i, \underline{\boldsymbol{\mu}}_i, \overline{\boldsymbol{\mu}}_i, \underline{\boldsymbol{\omega}}_i, \overline{\boldsymbol{\omega}}_i$ to 0 and $\tilde{\mathbf{q}}_i = -\mathbf{q}_i^l$, where $\mathbf{q}_i^l$ denotes the reactive load at bus i;

IDLE:

while $\tau_i < T_i$ **do**

  Receive $\tilde{\mathbf{P}}_j$ from the child buses $j \in C_i$;

  Receive $\underline{\boldsymbol{\omega}}_i, \overline{\boldsymbol{\omega}}_i$ from the neighboring buses $j \in \{\pi_i, C_i\}$;

end

AWAKE:

Measure local voltage magnitude $\mathbf{V}_i$ and active power flow on the in-coming line $\mathbf{P}_i$;

Calculate $\tilde{\mathbf{P}}_i$ and update dual variables $\underline{\boldsymbol{\mu}}_i, \overline{\boldsymbol{\mu}}_i, \underline{\boldsymbol{\omega}}_i, \overline{\boldsymbol{\omega}}_i$ according to (16);

Update $\tilde{\mathbf{q}}_i$ according to (26);

Project $\tilde{\mathbf{q}}_i$ onto the feasible region as (27) and apple $\mathbf{q}_i^{\text{act}}$ to bus i;

Measure $\mathbf{P}_i$ and calculate $\tilde{\mathbf{P}}_i$. Broadcast $\tilde{\mathbf{P}}_i$ to its parent bus π_i and $\underline{\boldsymbol{\omega}}_i, \overline{\boldsymbol{\omega}}_i$ to its neighboring buses $\{\pi_i, Ci\}$;

Set $\tau_i = 0$, get a new realized awaiting time period T_i and go to **IDLE**.

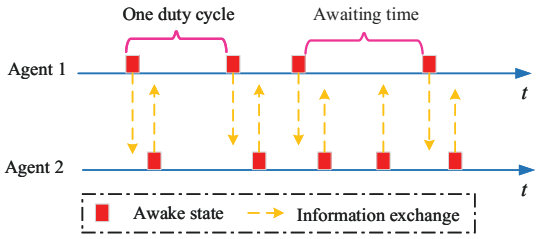

Fig. 1. Time line example of two agents using the asynchronous algorithm

independently. At idle state, each agent i only receives information from its neighbors. When the time elapsed τ_i exceeds the awaiting time threshold T_i, agent i enters into awake state and immediately measures its local voltage magnitude and real power flow on its incoming line. Then, it will calculate the intermediate variable $\tilde{\mathbf{P}}_i$ and update the dual variables. Next, the primal variable $\tilde{\mathbf{q}}_i$ will be updated and projected onto the feasible region before applying to bus i. Later, agent i will broadcast the relevant information to its neighbors and a new duty cycle begins by resetting τ_i.

The dual problem (30) can be reformulated as the following problem by converting the constraints to the indicator function and adding it to the objective function.

$$\min_{\mathbf{y}\in\mathbb{R}^m} \Gamma(\mathbf{y}) := -g(\mathbf{y}) + \Psi(\mathbf{y}) \tag{32}$$

where $\mathbf{y} = [\mathbf{y}_i^\top ... \mathbf{y}_N^\top]^\top$ and $m = N \times \dim(\mathbf{y}_i)$; $\Psi(\mathbf{y}) =: \sum_{i=1}^N \Psi_i(\mathbf{y}_i)$ and $\Psi_i(\mathbf{y}_i)$ is the indicator function of $\mathbf{y}_i$, i.e., $\Psi_i(\mathbf{y}_i) = 0$ if $\mathbf{y}_i \geq 0$ and $\Psi_i(\mathbf{y}_i) = +\infty$ otherwise.

Lemma 2. *The gradient of $g(\mathbf{y})$ is block coordinate-wise Lipschitz continuous with positive constant L_1,...L_N, i.e.,*

$$\|\nabla_i g(\mathbf{y} + \mathbf{W}_i \mathbf{s}_i) - \nabla_i g(\mathbf{y})\| \leq L_i \|\mathbf{s}_i\|$$

where $\nabla_i g(\mathbf{y})$ denote the i-th block component of $\nabla g(\mathbf{y})$; $\mathbf{W}_i$ is the i-th submatrix of $\mathbf{W} = [\mathbf{W}_1\ \mathbf{W}_2 ... \mathbf{W}_N]$ and $\mathbf{W}$ is a column permutation of $m \times m$ identity matrix.

Proof. According to equation (30), we have $\nabla g(\mathbf{y}) = -\mathbf{E}\mathbf{H}^{-1}\mathbf{E}^\top \mathbf{y} - \mathbf{E}\mathbf{H}^{-1}\mathbf{c} - \mathbf{b}$. Plugging it into $\|\nabla_i g(\mathbf{y} + \mathbf{W}_i \mathbf{s}_i) - \nabla_i g(\mathbf{y})\|$, we have

$$\begin{aligned}\|\nabla_i g(\mathbf{y} + \mathbf{W}_i \mathbf{s}_i) - \nabla_i g(\mathbf{y})\| &= \|\mathbf{W}_i^\top \mathbf{E}\mathbf{H}^{-1}\mathbf{E}^\top \mathbf{W}_i \mathbf{s}_i\| \\ &\leq \|\mathbf{W}_i^\top \mathbf{E}\mathbf{H}^{-1}\mathbf{E}^\top \mathbf{W}_i\| \|\mathbf{s}_i\|\end{aligned}$$

The inequality follows due to the definition of matrix norm. Hence, $L_i := \|\mathbf{W}_i^\top \mathbf{E}\mathbf{H}^{-1}\mathbf{E}^\top \mathbf{W}_i\|$. □

Assumption 1. *The awaiting time T_i of each agent i is an independent and identically distributed (i.i.d.) random variable with exponential probability distribution.*

Theorem 2. *Suppose that Assumption 1 holds and in Algorithm 1 each local step size α_i is chosen such that $0 < \alpha_i \leq 1/L_i$, where L_i is the Lipschitz constant for the i-th block of gradient $\nabla g(\mathbf{y})$. Then the sequences of dual variables $\mathbf{y}^k = [(\mathbf{y}_i^k)^\top ... (\mathbf{y}_N^k)^\top]^\top$ generated by Algorithm 1 converges to the optimal value with high probability. That is for any $\varepsilon \in (0, \Gamma(\mathbf{y}^0) - \Gamma^*)$, there exists $\bar{k}(\varepsilon, \rho) > 0$ such that for all $k > \bar{k}$ we have*

$$\Pr\big(\Gamma(\mathbf{y}^t) - \Gamma^* \leq \varepsilon\big) \geq 1 - \rho$$

where $\mathbf{y}^0$ is the initial value of dual variables, Γ^* is the optimal value of dual problem and ρ is the target confidence.

Proof. As illustrated in [30], three conditions need to be satisfied to establish the convergence of the proposed asynchronous algorithm, i.e., the block coordinate-wise Lipschitz continuity of the gradient of $-g(\mathbf{y})$, the separability of the function $\Psi(\mathbf{y})$ and the feasibility of problem (32). Lemma 2 and definition of $\Psi(\mathbf{y})$ ensure that conditions 1 and 2 are met in our application. Furthermore, since the primal problem (29) is a strictly convex quadratic programming with linear constraints, the strong duality holds [32]. Hence, the feasibility condition also holds and it suffices to show that the updating formula of $\mathbf{y}_i$ can be reformulated in the same format as in [30]. According to Theorem 1, the dual variables of each agent are updated as

$$\mathbf{y}_i^{k+1} = \big[\mathbf{y}_i^k + \alpha_i \nabla_i g(\mathbf{y}^k)\big]^+ \tag{33}$$

which is reformulated as

$$\mathbf{y}_i^{k+1} = \mathbf{prox}_{\alpha_i \Psi_i}\Big(\mathbf{y}_i^k + \alpha_i \nabla_i g(\mathbf{y}^k)\Big) \tag{34}$$

where $\mathbf{prox}_{\alpha_i \Psi_i}(\mathbf{y})$ denotes the proximal operator. Since (34) has the same format as the updating formula in [30], the theorem is proven by following the same arguments as in [30, Theorem V.14].

□

IV. Numerical Results

The proposed synchronous and asynchronous distributed online voltage control algorithms - denoted as **Dist-S** and **Dist-A**, respectively - are tested on the three-phase unbalanced

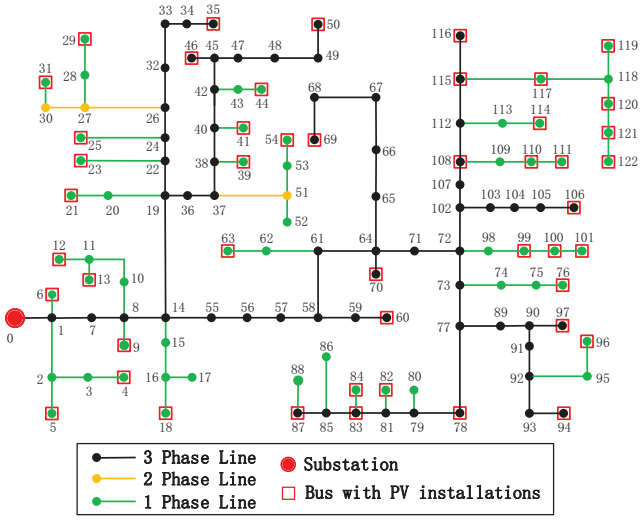

Fig. 2. IEEE 123-bus distribution system with PV installations

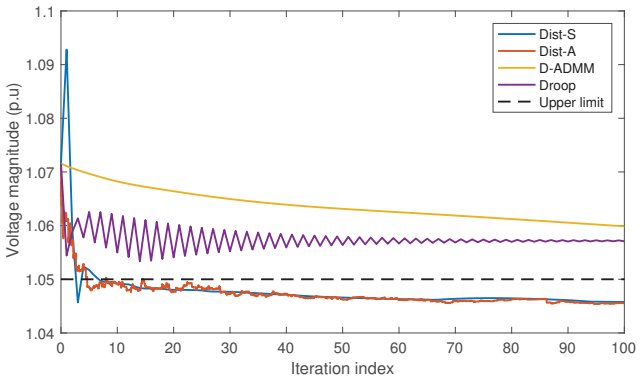

Fig. 3. Convergence of the maximum nodal voltage magnitude for case 1

IEEE 123-bus DN shown in Fig. 2. The line parameters and the load data can be accessed from [33]. The base voltage is 4.16 kV and the voltage magnitudes in the case studies are expressed in the per-unit values. The locations of PV installations are indicated in Fig. 2. The generation capacity and rated apparent power of each PV system are set as 200 kW and 1.05 $\times$ 200 kVA, respectively. Three cases are considered to verify the effectiveness of our proposed algorithms. In the first case, the performance of Dist-S and Dist-A are compared with four benchmark approaches. In the second one, we validate the robustness of Dist-S against the communication failures. The third case corroborates the effectiveness of Dist-S and Dist-A under the dynamic system operating conditions. In all case studies, the actual bus voltage magnitudes and the active power flows on the incoming lines obtained from local measurements, are used to update the primal and dual variables. The lower and upper limits for nodal voltage magnitude are 0.95 and 1.05 p.u. respectively. All tests are performed using MATLAB on a personal computer with an Intel Core i7 of 2.5GHz and 16GB memory.

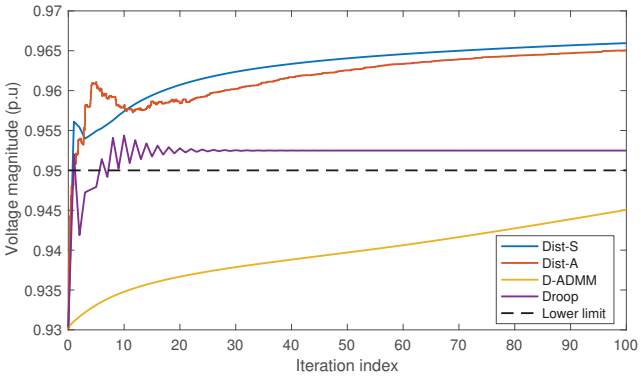

Fig. 4. Convergence of the minimum nodal voltage magnitude for case 2

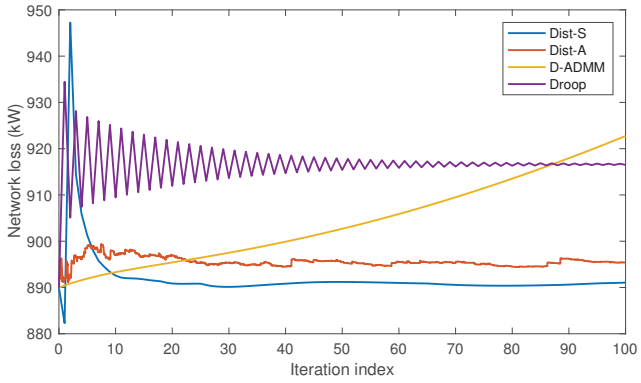

Fig. 5. Convergence of the network loss for case 1

A. *Performance Comparisons*

In this subsection, we compare the performance of our proposed algorithms with four other benchmark approaches. The first one is the standard form of linear Q-V droop method, denoted as Droop. The second one is a recently proposed ADMM based distributed online VAR control strategy (D-ADMM) [19] which is designed for reducing the voltage deviations from the nominal value. Two centralized strategies (Cen-linear & Cen-SDP) are also adopted to verify the optimal performance of our proposed algorithms, where Cen-linear is to solve problem (14) in a centralized manner and Cen-SDP solves a SDP problem converted from the fully nonlinear AC OPF problem by relaxing the rank-one constraints [21]. To make comprehensive comparisons, two representative static cases are considered, namely **case 1** and **case 2**. Specifically, case 1 often occurs at noon when PV generation is high (95% of the peak capacity) and load consumption is low (60% of the peak load), and thus resulting in over-voltage violations; In contrast, case 2 often occurs at early night when PV generation is not available and load consumption is high (peak load), and thereby giving rise to under-voltage violations.

Since in Dist-A different buses updates their control variables asynchronously, the count of iterations is redefined such that one iteration contains the same number of updates with the synchronous algorithm. In particular, the count of iteration increases by 1 whenever 122 updates are completed. The awaiting time T_i of each agent in Dist-A is assumed

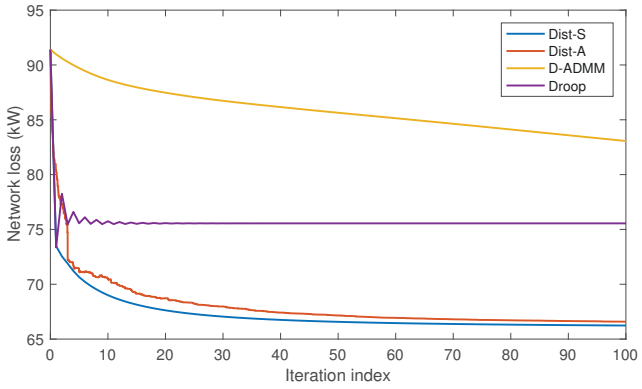

Fig. 6. Convergence of the network loss for case 2

to follow the i.i.d. exponential distribution and the mean of T_i is set as 3 seconds without loss of generality. Figs. 3 and 4 show the convergence of the maximum and minimum nodal voltage magnitudes using different approaches for cases 1 and 2, respectively. It can be seen from the figures that the curves of Dist-A are more rugged than those of Dist-S due to the randomized updates of different agents. Besides, prior to the deployment of VAR control, severe over-voltage and under-voltage violations are observed in cases 1 and 2, respectively. Although the Droop method mitigates the voltage violations to some extent, it fails to eliminate the over-voltage violations in case 1 as shown in Fig. 3, due to the lack of coordination between different PV units, especially when the VAR resources are insufficient. For D-ADMM strategy, both the maximum voltage magnitude in case 1 and the minimum voltage magnitude in case 2 converge very slowly and are still beyond the limits after 100 iterations. The reason is that the design of the D-ADMM aiming at reducing voltage deviations, does not consider the voltage constraints and hence is unable to incorporate the information of voltage violations. In contrast, our proposed Dist-S and Dist-A remove all voltage violations rapidly with just a few iterations, which validates the advantage of our proposed algorithms in voltage regulation over the Droop and D-ADMM strategies.

Figs. 5 and 6 depict the convergence of network loss using different approaches for cases 1 and 2, respectively. It can be observed in these figures that using Dist-S algorithm, the network losses converge to the smallest values in both cases, while the converged network losses using Dist-A algorithm, are slightly higher. It will be shown in the following that their converged values are nearly global optimal. Using the Droop method, the network losses have much higher oscillations compared to those using Dist-S algorithm. Finally, the network losses using D-ADMM method are higher than those using Dist-S and Dist-A algorithms as loss minimization is not considered in D-ADMM method. Hence, our proposed Dist-S and Dist-A algorithms outperform Droop and D-ADMM methods in terms of loss minimization.

To substantiate the optimality of our proposed distributed algorithms, we also compare their converged results with two centralized approaches, i.e, Cen-linear and Cen-SDP. Table I summarizes the network losses using our approaches and

TABLE I
NETWORK LOSSES USING THE PROPOSED ALGORITHMS AND TWO CENTRALIZED APPROACHES

Methods	Case1		Case2	
	Loss/kW	Ratio	Loss/kW	Ratio
Dist-S	891.2	1.007	66.1	1.003
Dist-A	894.5	1.011	66.4	1.008
Cen-linear	977.8	1.105	66.1	1.003
Cen-SDP	885.1	1.000	65.9	1.000

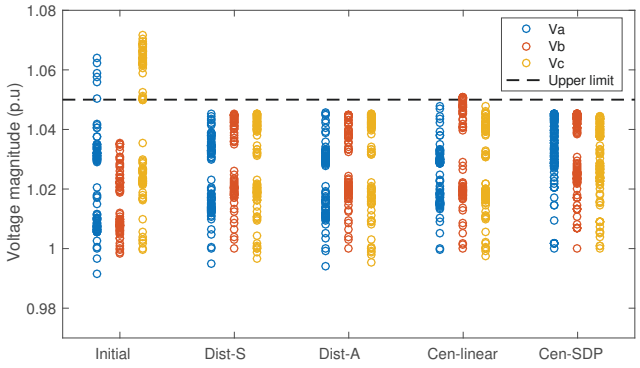

Fig. 7. Distributions of nodal voltage magnitudes using different methods for case 1

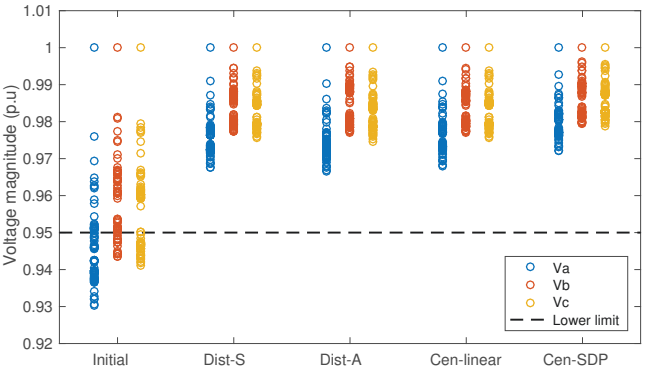

Fig. 8. Distributions of nodal voltage magnitudes using different methods for case 2

two centralized strategies. As shown in this table, in both cases Cen-SDP achieves the lowest network losses. However, since Cen-SDP relaxes the rank-one constraints in the original fully nonlinear AC OPF problem, the resulting optimal value represents a lower bound of the minimal loss, which may not be attained in practice. Here, the network losses caused by Dist-S and Dist-A are just slightly higher (0.3%-1.1%) than the global lower bound, which verifies the near global optimality of our proposed algorithms. Note that even though Cen-SDP yields the smallest network loss, it can hardly be used for real-time voltage control in practice due to the considerable computational and communication burdens. Moreover, it is worth noting that the network loss using Cen-linear method is higher than those using Dist-S and Dist-A approaches in case 1, even though the latter two are developed using the same model as Cen-linear. The difference is caused by the model mismatch of the linearized power flow equations and

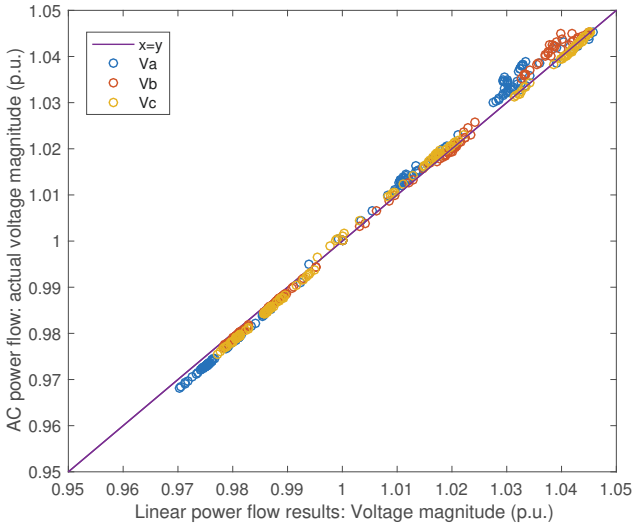

Fig. 9. Correlation between the estimated voltage magnitudes from the linear power flow model and the actual voltage magnitudes from the nonlinear AC power flow model

the approximation error in nodal voltage and power flows. Using Cen-linear method, the power flow is approximated by the linear model; however, Dist-S and Dist-A methods use the nodal voltage magnitudes and line flows obtained from local measurements to update the control variables. Consequently, the adverse impact of model mismatch is mitigated using Dist-S and Dist-A methods.

Figs. 7 and 8 show the distributions of three-phase voltages under different methods for Cases 1 and 2, respectively. As shown in these figures, the voltage distributions are quite similar in case 2 using Cen-linear, Dist-S and Dist-A methods; however, in case 1 the voltage distribution using Cen-linear method is slightly different with those using Dist-S and Dist-A approaches. Besides, in case 2, Cen-linear method fails to eliminate all voltage violations due to the approximation error in the model. Note that since the relaxation of the rank-constraints is not exact in Cen-SDP approach, its voltage distributions are quite different with other three approaches. Fig. 9 depicts the correlation between the estimated voltage magnitudes derived from the linear power flow model and the actual voltage magnitudes. This figure shows that the estimated voltage magnitudes and the actual ones are closely correlated and the approximation error grows as the voltage deviation increases.

B. Robustness

To validate the robustness of our proposed algorithms, case studies with communication interruptions are carried out. Since Dist-A is an asynchronous algorithm that takes communication delays into consideration, it is inherently robust against communication interruptions. Hence, we only need to validate the robustness of Dist-S algorithm. It is assumed that the communication interruptions, e.g., packet drop, occur randomly between any two neighboring agents with a probability ρ. Tables II and III ummarize the statistical voltage magnitude and network loss measures with 20 iterations of

TABLE II
STATISTICAL VOLTAGE MAGNITUDE AND NETWORK LOSS MEASURES WITH DIST-S ALGORITHM CONSIDERING COMMUNICATION INTERRUPTIONS FOR CASE 1

Probability ρ	maximum voltage magnitude/p.u. mean (std)	Loss/kW mean (std)
0	1.048 (0)	891.8 (0)
0.1	1.048 (8.4×10^{-5})	891.9 (0.083)
0.2	1.048 (1.0×10^{-4})	892.0 (0.105)
0.3	1.048 (1.2×10^{-4})	892.1 (0.126)
0.4	1.048 (1.3×10^{-4})	892.2 (0.129)

TABLE III
STATISTICAL VOLTAGE MAGNITUDE AND NETWORK LOSS MEASURES WITH DIST-S ALGORITHM CONSIDERING COMMUNICATION INTERRUPTIONS FOR CASE 2

Probability ρ	minimum voltage magnitude/p.u. mean (std)	Loss/kW mean (std)
0	0.961 (0)	67.6 (0)
0.1	0.961 (5.2×10^{-5})	67.8 (0.012)
0.2	0.960 (7.1×10^{-5})	67.9 (0.017)
0.3	0.960 (8.1×10^{-5})	68.0 (0.019)
0.4	0.960 (8.2×10^{-5})	68.1 (0.020)

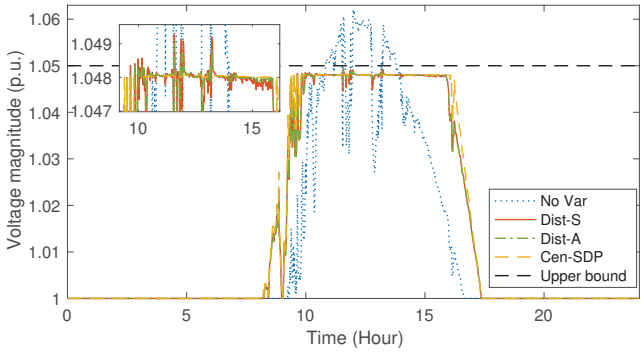

Fig. 10. Daily profiles of maximum nodal voltage magnitudes under different methods

Dist-S algorithm for cases 1 and 2, respectively. Here, the scenarios with $\rho = 0$ represent perfect communication, which are used as benchmarks. For other scenarios, the simulation is performed 1000 times to obtain the statistical outputs. As can be observed from the tables, both the network loss and voltage magnitudes change marginally with the increase in the rate of communication loss. Therefore, our proposed Dist-S is robust against communication failures.

C. Dynamic Operation Cases

The proposed algorithms are exposed to the dynamic system operating conditions that capture the variations of demand and PV generations. The voltage control is carried out for an entire day using the same minutely load and PV data as [18]. We assume within each minute the loads and PV outputs are constant. In Dist-S algorithm, the duration of one duty cycle is set to 3 seconds, and in Dist-A algorithm, the waiting time for each agent is randomly generated from a uniform distribution ranging from 2.5 to 3.5 seconds. The simulation results are

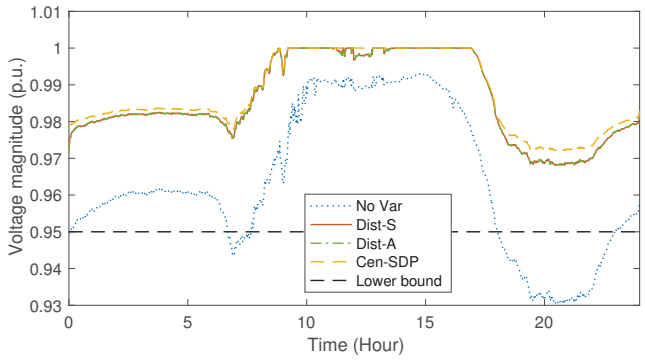

Fig. 11. Daily profiles of minimum nodal voltage magnitudes under different methods

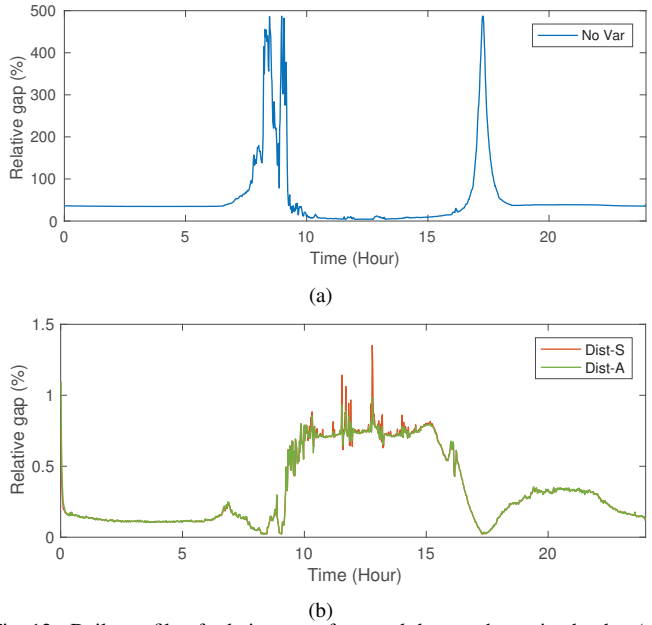

Fig. 12. Daily profile of relative gap of network loss to the optimal value (a) no VAR control (b) Dist-S and Dist-A

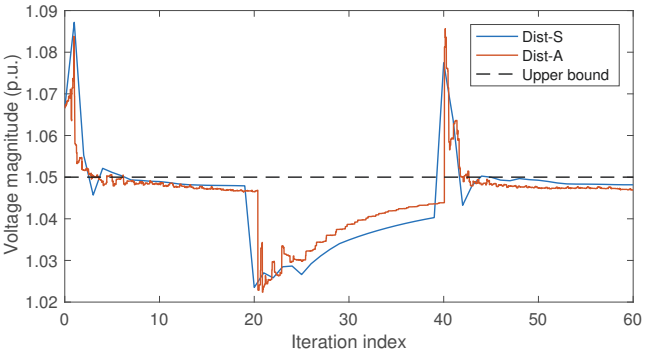

Fig. 13. Profiles of maximum nodal voltage magnitudes with the sudden disturbance of PV generations

compared with those procured by using Cen-SDP algorithm to verify the solution quality of our proposed algorithms under the variation of system operating conditions. The scenario without VAR control is also considered as a benchmark. Figs. 10 and 11 depict the daily maximum and minimum nodal voltage profiles using different VAR control methods, respectively. It is shown that without VAR control the DN would suffer from severe under-voltage violations during evening and over-voltage violations at noon. When Dist-S and Dist-A algorithms are applied, all voltage violations are mitigated efficiently. Fig. 12 plots the relative gaps between the network loss provided by Cen-SDP algorithm and those provided by Dist-A and Dist-S algorithms. It is shown that our proposed algorithms achieve the minimum network loss as the relative gaps are always below 1.5%. Furthermore, significant loss reduction can be achieved by invoking our proposed algorithms as the network loss without VAR control is considerably large. Therefore, the proposed Dist-S and Dist-A algorithms are efficient in regulating voltages and minimizing network loss under the dynamically varying system operating conditions.

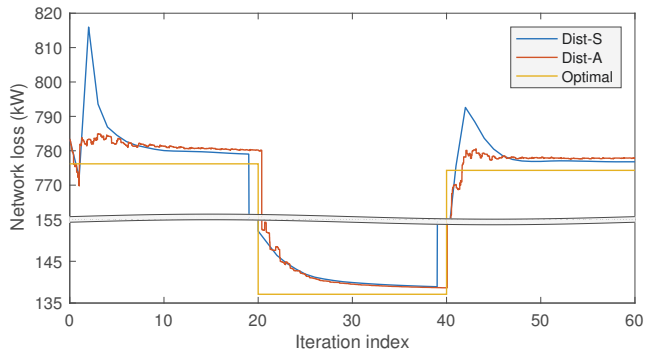

Fig. 14. Profiles of network loss with the sudden disturbance of PV generations

The proposed algorithms are also tested in the scenario with sudden disturbance of PV generation. Fig. 13 shows the maximum nodal voltage magnitudes when 50% of the PV generation is lost at the 20th iteration and recovered at the 40th iteration. As shown in this figure, the sudden change of PV generation leads to the substantial variations of voltage magnitudes and sometimes even cause voltage violations. Nevertheless, both Dist-S and Dist-A algorithms can quickly restore the voltages within the feasible ranges. Fig. 14 plots the profiles of the network loss with the sudden disturbance of PV generation. The global minimal values derived using Cen-SDP algorithm are also demonstrated in this figure. It is shown that the network losses using Dist-S and Dist-A algorithms trace the global minimum with a very fast speed even under the significant variations of system operating conditions.

D. Discussion

In subsection IV-A, the performance of our proposed Dist-S and Dist-A is compared with two benchmark approaches, i.e. Droop and D-ADMM. The results indicate that Dist-S and Dist-A algorithms are more efficient than Droop and D-ADMM in eliminating voltage violations and minimizing network loss because Dist-S and Dist-A algorithms fully exploit the system-wide information for the updates of control variables. Then, the optimality of the solutions provided by Dist-S and Dist-A algorithms are validated by comparing them

with those procured by two centralized approaches. The case studies show that the results procured by implementing Dist-A algorithm are just slightly different with those procured by using Dist-S algorithm. This validates the effectiveness of the Dist-A algorithm.

In subsection IV-B, the robustness of Dist-S algorithm is validated against communication interruptions. Whenever the communication loss occurs between two adjacent agents, they will use the previously received information to update their control variables. It is shown that the communication failure has limited influence on the results.

In subsection IV-C, to account for the online application, Dist-S and Dist-A algorithms are tested for the cases with fast variations in system operating conditions. The results show that the performance of Dist-S and Dist-A algorithms are comparable with an ideal centralized approach. Moreover, it is shown that Dist-S and Dist-A algorithms can efficiently handle the sudden disturbances in PV generation.

In summary, Dist-S and Dist-A algorithms are effective for online voltage control. The former suits the applications when a global time exists to trigger the updates for different agents, and the latter is more applicable in practice considering the communication delays.

V. Conclusions

In this paper, two distributed online voltage control algorithms are proposed. Different from most existing voltage control algorithms, the proposed algorithms are designed for multiphase unbalanced DNs and enable online implementation to adapt to the fast-varying system operating conditions. Firstly, we formulate the voltage control problem as a convex quadratic programming by adopting the linearized multiphase DistFlow model. Then, the dual ascent method is applied to derive the synchronous distributed algorithm with closed-form solutions for optimization subproblems. Furthermore, we significantly reduce communication complexity to the extent that only neighborhood communication is required. To deal with the communication asynchrony, an asynchronous version of the distributed algorithm is developed. Numerical results on the IEEE 123-bus DN validate the effectiveness of the proposed algorithms and demonstrate the improved performance compared with other methods.

References

[1] Y. Zhang, J. Wang, and Z. Li, "Uncertainty modeling of distributed energy resources: techniques and challenges," *Current Sustainable/Renewable Energy Reports*, vol. 6, no. 2, pp. 42–51, 2019.

[2] C. Wan, J. Lin, J. Wang, Y. Song, and Z. Y. Dong, "Direct quantile regression for nonparametric probabilistic forecasting of wind power generation," *IEEE Transactions on Power Systems*, vol. 32, no. 4, pp. 2767–2778, 2016.

[3] H. R. Baghaee, M. Mirsalim, G. B. Gharehpetan, and H. A. Talebi, "Nonlinear load sharing and voltage compensation of microgrids based on harmonic power-flow calculations using radial basis function neural networks," *IEEE systems journal*, vol. 12, no. 3, pp. 2749–2759, 2017.

[4] E. Dall'Anese, S. V. Dhople, and G. B. Giannakis, "Optimal dispatch of photovoltaic inverters in residential distribution systems," *IEEE Transactions on Sustainable Energy*, vol. 5, no. 2, pp. 487–497, 2014.

[5] H. Zhu and H. J. Liu, "Fast local voltage control under limited reactive power: Optimality and stability analysis," *IEEE Transactions on Power Systems*, vol. 31, no. 5, pp. 3794–3803, 2016.

[6] C. Zhang and Y. Xu, "Hierarchically-coordinated voltage/var control of distribution networks using pv inverters," *IEEE Transactions on Smart Grid*, 2020.

[7] H.-G. Yeh, D. F. Gayme, and S. H. Low, "Adaptive var control for distribution circuits with photovoltaic generators," *IEEE Transactions on Power Systems*, vol. 27, no. 3, pp. 1656–1663, 2012.

[8] R. A. Jabr, "Radial distribution load flow using conic programming," *IEEE transactions on power systems*, vol. 21, no. 3, pp. 1458–1459, 2006.

[9] M. Farivar and S. H. Low, "Branch flow model: Relaxations and convexificationpart i," *IEEE Transactions on Power Systems*, vol. 28, no. 3, pp. 2554–2564, 2013.

[10] K. E. Antoniadou-Plytaria, I. N. Kouveliotis-Lysikatos, P. S. Georgilakis, and N. D. Hatziargyriou, "Distributed and decentralized voltage control of smart distribution networks: Models, methods, and future research," *IEEE Transactions on smart grid*, vol. 8, no. 6, pp. 2999–3008, 2017.

[11] E. Dall'Anese, H. Zhu, and G. B. Giannakis, "Distributed optimal power flow for smart microgrids," *IEEE Transactions on Smart Grid*, vol. 4, no. 3, pp. 1464–1475, 2013.

[12] Q. Peng and S. H. Low, "Distributed optimal power flow algorithm for radial networks, i: Balanced single phase case," *IEEE Transactions on Smart Grid*, vol. 9, no. 1, pp. 111–121, 2016.

[13] P. Li, C. Zhang, Z. Wu, Y. Xu, M. Hu, and Z. Dong, "Distributed adaptive robust voltage/var control with network partition in active distribution networks," *IEEE Transactions on Smart Grid*, 2019.

[14] Z. Tang, D. J. Hill, and T. Liu, "Fast distributed reactive power control for voltage regulation in distribution networks," *IEEE Transactions on Power Systems*, vol. 34, no. 1, pp. 802–805, 2018.

[15] P. Šulc, S. Backhaus, and M. Chertkov, "Optimal distributed control of reactive power via the alternating direction method of multipliers," *IEEE Transactions on Energy Conversion*, vol. 29, no. 4, pp. 968–977, 2014.

[16] W. Zheng, W. Wu, B. Zhang, H. Sun, and Y. Liu, "A fully distributed reactive power optimization and control method for active distribution networks," *IEEE Transactions on Smart Grid*, vol. 7, no. 2, pp. 1021–1033, 2016.

[17] S. Bolognani, R. Carli, G. Cavraro, and S. Zampieri, "Distributed reactive power feedback control for voltage regulation and loss minimization," *IEEE Transactions on Automatic Control*, vol. 60, no. 4, pp. 966–981, 2014.

[18] J. Li, Z. Xu, J. Zhao, and C. Zhang, "Distributed online voltage control in active distribution networks considering pv curtailment," *IEEE Transactions on Industrial Informatics*, vol. 15, no. 10, pp. 5519–5530, 2019.

[19] H. J. Liu, W. Shi, and H. Zhu, "Distributed voltage control in distribution networks: Online and robust implementations," *IEEE Transactions on Smart Grid*, vol. 9, no. 6, pp. 6106–6117, 2017.

[20] W. H. Kersting, *Distribution System Modeling and Analysis*. CRC Press, 2017.

[21] L. Gan and S. H. Low, "Convex relaxations and linear approximation for optimal power flow in multiphase radial networks," in *2014 Power Systems Computation Conference*. IEEE, 2014, pp. 1–9.

[22] V. Kekatos, L. Zhang, G. B. Giannakis, and R. Baldick, "Voltage regulation algorithms for multiphase power distribution grids," *IEEE Transactions on Power Systems*, vol. 31, no. 5, pp. 3913–3923, 2015.

[23] B. A. Robbins and A. D. Domínguez-García, "Optimal reactive power dispatch for voltage regulation in unbalanced distribution systems," *IEEE Transactions on Power Systems*, vol. 31, no. 4, pp. 2903–2913, 2015.

[24] X. Zhou, Z. Liu, C. Zhao, and L. Chen, "Accelerated voltage regulation in multi-phase distribution networks based on hierarchical distributed algorithm," *IEEE Transactions on Power Systems*, 2019.

[25] S. M. Mohiuddin and J. Qi, "Droop-free distributed control for ac microgrids with precisely regulated voltage variance and admissible voltage profile guarantees," *IEEE Transactions on Smart Grid*, 2019.

[26] J. Xu, H. Sun, and C. J. Dent, "Admm-based distributed opf problem meets stochastic communication delay," *IEEE Transactions on Smart Grid*, 2018.

[27] T. Zhao, Z. Li, and Z. Ding, "Consensus-based distributed optimal energy management with less communication in a microgrid," *IEEE Transactions on Industrial Informatics*, 2018.

[28] J. Zhang, S. Nabavi, A. Chakrabortty, and Y. Xin, "Admm optimization strategies for wide-area oscillation monitoring in power systems under asynchronous communication delays," *IEEE Transactions on Smart Grid*, vol. 7, no. 4, pp. 2123–2133, 2016.

[29] J. Mohammadi, G. Hug, and S. Kar, "Agent-based distributed security constrained optimal power flow," *IEEE Transactions on Smart Grid*, vol. 9, no. 2, pp. 1118–1130, 2016.

[30] I. Notarnicola and G. Notarstefano, "Asynchronous distributed optimization via randomized dual proximal gradient," *IEEE Transactions on Automatic Control*, vol. 62, no. 5, pp. 2095–2106, 2016.
[31] D. P. Bertsekas, *Nonlinear programming*. Athena scientific Belmont, 1999.
[32] S. Boyd and L. Vandenberghe, *Convex optimization*. Cambridge university press, 2004.
[33] D. T. F. W. Group *et al.*, "Distribution test feeders," *Available from: http://sites.ieee.org/pes-testfeeders/resources*, 2010.

Jiayong Li (S'16-M19) received the B.Eng. degree from Zhejiang University, Hangzhou, China, in 2014, and the Ph.D. degree from The Hong Kong Polytechnic University, Hong Kong, in 2018. He joined the the College of Electrical and Information Engineering of Hunan University as an Assistant Professor in 2019. He is currently a Post Doctoral Fellow with the Department of Electrical and Computer Engineering, Southern Methodist University, Dallas, TX, USA. He was a Postdoctoral Research Fellow with The Hong Kong Polytechnic University and a Visiting Scholar with Argonne National Laboratory, Argonne, IL, USA. His research interests include distribution system planning and operation, power economics, demand-side energy management, and distributed control.

Chengying Liu received the B.Eng. degree in electrical engineering and automation from Yanshan University, Qinhuangdao, China, in 2019. She is currently pursuing the M.Sc. degree at Hunan University, Changsha, China. Her current research interests include energy management, and distribution system operation.

Mohammad E. Khodayar (SM17) received the B.Sc. degree in electrical engineering from the Amirkabir University of Technology, Tehran, Iran, the M.S. degree in electrical engineering from the Sharif University of Technology, Tehran, and the Ph.D. degree in electrical engineering from the Illinois Institute of Technology, Chicago, IL, USA, in 2012. He was a Senior Research Associate with the Robert W. Galvin Center for Electricity Innovation, Illinois Institute of Technology. He is currently an Associate Professor with the Department of Electrical Engineering, Southern Methodist University, Dallas, TX, USA. His research interests include power system operation and planning. He is an Associate Editor of the IEEE TRANSACTIONS ON SUSTAINABLE ENERGY and the IEEE TRANSACTIONS ON VEHICULAR TECHNOLOGY.

Ming-Hao Wang (S15-M18) received the B.Eng.(Hons.) degree in electrical and electronic engineering from the Huazhong University of Science and Technology, Wuhan, China, and the University of Birmingham, Birmingham, U.K. in 2012, and the M.Sc. and the Ph.D. degree, both in electrical and electronic engineering, from The University of Hong Kong, Hong Kong, in 2013 and 2017, respectively. Since 2018, he has been with the Department of Electrical Engineering, Hong Kong Polytechnic University, Hong Kong. Currently, he is a Research Assistant Professor in the Department of Electrical Engineering, the Hong Kong Polytechnic University. His search interests include power systems and power electronics.

Zhao Xu (M'06-SM'12) received B.Eng, M.Eng and Ph.D degree from Zhejiang University, National University of Singapore, and The University of Queensland in 1996, 2002 and 2006, respectively. From 2006 to 2009, he was an Assistant and later Associate Professor with the Centre for Electric Technology, Technical University of Denmark, Lyngby, Denmark. Since 2010, he has been with The Hong Kong Polytechnic University, where he is currently a Professor in the Department of Electrical Engineering and Leader of Smart Grid Research Area. He is also a foreign Associate Staff of Centre for Electric Technology, Technical University of Denmark.

His research interests include demand side, grid integration of wind and solar power, electricity market planning and management, and AI applications. He is an Editor of the Electric Power Components and Systems, the IEEE PES Power Engineering Letter, and the IEEE Transactions on Smart Grid. He is currently the Chairman of IEEE PES/IES/PELS/IAS Joint Chapter in Hong Kong Section.

Bin Zhou (S11-M13-SM17)) was born in Hunan Province, China, in 1984. He received the B.Sc. degree in electrical engineering from Zhengzhou University, Zhengzhou, China, in 2006, the M.S. degree in electrical engineering from South China University of Technology, Guangzhou, China, in 2009, and the Ph.D. degree from The Hong Kong Polytechnic University, Hong Kong, in 2013. Afterwards, he worked as a Research Associate and subsequently a Postdoctoral Fellow in the Department of Electrical Engineering of The Hong Kong Polytechnic University. Now, he is an Associate Professor in the College of Electrical and Information Engineering, Hunan University, Changsha, China. His main fields of research include smart grid operation and planning, renewable energy generation, and energy efficiency.

Canbing Li (M06-SM13) received the B.Sc. and Ph.D. degrees both in electrical engineering from Tsinghua University, Beijing, China, in 2001 and 2006, respectively. He is currently a Professor with Department of Electrical Engineering, Shanghai Jiao Tong University, Shanghai, China. His research interests include smart grid, energy efficiency, and energy policy.